

# **Review: PEMFC Materials' Thermal Conductivity and Influence on Internal Temperature Profiles**

Odne S. Burheim<sup>a</sup>

<sup>a</sup>Dep. of Energy and Process Engineering, NTNU, Norway

The polymer electrolyte membrane fuel cell (PEMFC) is far from isothermal when in operation. This is well established both from experiments and from mathematical modelling. Over the last 15 years, the research field and knowledge about thermal conductivity and heat generation in the PEMFC materials has been established and developed. From first looking at through-plane thermal conductivity of only membranes and gas diffusion layers (GDL), the most recent studies include heat transport properties on non-isotropic properties, PTFE content, water content, compression, heat pipe effects, and material integration. This short review explains the knowledge development within the field of thermal conductivity of PEMFC materials and regions over the last 15 years. It also shows how this knowledge changes our understanding of internal temperature profiles in a PEMFC under operation using a 2D- continuum based thermal model.

## **Introduction**

The polymer electrolyte membrane fuel cell (PEMFC) has developed in to a very effective converter of hydrogen to power. Effective in this context means that it is has had its reaction rate per membrane area developed. The energy efficiency, however, remains constant. In this way it is fair to state that the PEMFC has increased its effectiveness rather than efficiency.

The efficiency remains constant because the operation cell voltage remains constant. Even when the sources for irreversible energy dissipation improves, the operation cell voltage remains, typically ranging 0.6-0.8 V. Improved kinetics has lead to increased conversion rates and power density. Considering that there are commercial PEMFC systems of 100 kW weighing less than 100 kg, the power density even succeed Li-ion batteries (1). Yet the price remains areas for improvement.

Efficiency with respect to electric energy sees its reduction from particularly two sources of friction; Ohmic potential loss (friction of passing charge through the cell) and Tafel over-

potential (friction of transferring electrons between catalyst and reactant (2)). Reducing the ohmic resistance by a factor of two and double the exchange current density (improved Tafel kinetics) at 0.6 V will close to double the current density, the power density, and also the heat density (3). Thus more heat and power are both outcomes of a more effective PEMFC.

Improved performance of a PEMFC thus means increased heat development. Therefore, PEMFC development more and more leads to a need for including non-isothermal considerations alongside heat management. This is for several reasons. For instance, it is experimentally demonstrated that there is a strong correlation between local degradation and local temperature profiles (4), although PEMFCs are shown to last for 26 000 hours (3 years) continuous operation (5). In order to investigate this and similar effects further, detailed knowledge about local heat production, local thermal conductivity, thermo-mechanical stress, etc. is required. Kandlikar and Li summarise this in 2009 (6) by discussing literature available at the time and presenting a thermal model accordingly. Bapat and Thynell gave a separate review on thermal PEMFC modelling already in 2007 (7). Since then several developments of the available knowledge of PEMFC thermal conductivity has emerged. Thermal conductivity is an intrinsic property of the materials in a PEMFC and dictates the temperature distribution once the geometry and heat sources are known. Overview of the thermal conductivity of PEMFC materials and components is therefore important for engineering and scientific studies of the PEMFC.

Zamel and Li gave an extensive overview on PEMFC mechanical properties - also including thermal conductivity (8), but even over the last five years the knowledge and understanding of PEMFC materials thermal conductivity has progressed. This paper aims to line out the history of PEMFC thermal conductivity and also to use a relevant and simple model to illustrate how the knowledge affects possible understandings of temperature distribution in a PEMFC under stationary operation. The review is narrow in the way that it focus mainly on the knowledge gained for PEMFC thermal conductivity.

### **PEMFC Thermal Conductivity Overview**

Several different components constitute a PEMFC, *i.e.* the Membrane Electrolyte Assembly (MEA) sandwiched between a thin Micro Porous Layer (MPL) and a somewhat thicker Gas Diffusion Layer (GDL). The MEA, in turn, consists of a membrane coated with catalyst layers, CL, on each side. Additionally, there is an overlap between the MPL and the GDL which traditionally is given very little attention. A sketch of the PEMFC and all the relevant regions is given Fig. 1, in the model description section. This figure indicates the difference with (right) and without (left) the GDL-MPL overlap region. All of these regions have different properties and in some regions, like for the GDL, a great variety of materials with very different properties are available. Over the last decade, several efforts have lead to more knowledge about the thermal conductivity of these materials. An outline of the thermal conductivity knowledge progression is given after a brief introduction to the applied techniques for determining thermal conductivity.

## Thermal Conductivity Measurement Techniques

Because of the porosity, compressibility, and anisotropy of the PEMFC components, particularly the GDL, a standard laser flash technique (LFT) instrument will not suit the measurements needs. In fact, GDLs are so porous that they can be partly transparent. A laser beam will this partly go through the material. Moreover, in the cases where one is interested addition of water or even include a combination of water and x-ray computer aided tomography, the samples must be shielded from uncontrolled dry-out. A laser flash heats one small region, in turn inducing dry outs or phase induced mass flow. Because of this, other techniques than the LFT are tailored and developed. The denominator is to set up a determined heat flux, measure the temperature drop across the sample, and based on this information determine the thermal conductivity or resistivity.

Thermo-couple insertion into the fuel cell during operation is an early on applied technique for thermal conductivity measurements(9). The principle is to have thermocouples inserted several places in the PEMFC and measure actual temperature differences during operation. By calculating the heat production from cell potential and current density and using knowledge of the distance between the thermocouples allows for thermal conductivity estimates. While the strength of this technique is that it relates to rather real operational conditions, the allocation of the thermocouples leads to  $\pm 50\%$  deviation in the obtained values. This method is also only suited for through-plane thermal conductivity values.

The heat flux method can be applied for both through-plane and in-plane thermal conductivity values. Historically, this method was developed as one saw a need to determine through-plane thermal conductivity more accurately. Later one wanted to study the in-plane thermal conductivity, and in-plane thermal conductivity measurement devices were developed, however not with the capability of capturing compression and hydration effects. The through-plane heat flux method consists of applying two pistons with the sample in between. A known heat flux is set up and as the temperature drop, thickness and compression pressure (force) is reported. Stacking different amounts of samples allows for the subject material thermal conductivity to be separated from the contact to the pistons. The in-plane heat flux method consists of clamping a material sheet one two ends and sending the heat in-plane of this sheet. Measuring the distance and temperature drop thus gives the in-plane thermal conductivity from Fourier's law.

## Thermal Conductivity Values

A historical development of the knowledge in the field of thermal conductivity follows first, before a more detailed explanation of the context and experimental background follows.

Thermal Conductivity Knowledge Development in Brief A brief historical development of the thermal conductivity knowledge follows:

- i Vie and Kjelstrup were among the first to report thermal conductivities for PEMFC

components using the thermocouple insertion approach (9).

- ii Khandelwal and Mench reported thermal conductivity based on measured resistivity and uncompressed thickness for GDLs and dry Nafion at different compaction pressures using a heat flux method (Toray and SGL) (10).
- iii Ramousse *et al.* reported thermal conductivity based on measured resistivity and uncompressed thickness for GDLs (Quintech and SGL) and the contact to the apparatus (11). They addressed the problem of linearity when of stacking similar samples, *i.e.* that one has more unknown resistances than equations to solve the circuitry problem.
- iv Burheim *et al.* later found a way to separate the contact resistance between the measurement apparatus. (12, 13) Also, they were able to study and differentiate between apparatus sample and sample-sample thermal resistance. Including thickness measurements during compression was included for the first time.
- v Including liquid water in the GDLs was reported for the first time (13). It was measured how water changes the thermal conductivity several of these materials; Toray, Sigracet-SGL, Freudenberg, Solvicore, ETEK-ELAT, and Nafion (12, 13).
- vi The next important knowledge development was in-plane thermal conductivity (14–17). Depending on the compaction pressure, The difference between in-plane and through-plane thermal conductivity was readily proposed and interpreted in thermal models because it is like this also for the electric conductivity (18).
- vii The next issue that was investigated was the thermal conductivity of the MPL on top of GDLs (19–21), self standing MPLS (22), and the effect of accounting for different compactions of MPL and GDL (23).
- viii The last PEMFC region thermal conductivity to be investigated is the CL (24).
- ix Recently, studies investigating humidity cycling and its effect on GDL thermal conductivity has been undertaken to understand the dynamics of thermal conductivity in dynamic operation (25, 26)

It is the knowledge from the first 2 points that were available to Kandlikar and Li (6) and Bapat and Thynell (7). The knowledge from the first 5 points were available to Zamel and Li (8).

Thermal Conductivity Detailed Overview. Reliable measurements of the thermal conductivity of PEMFC materials is important and at the same time challenging. The water content, compaction pressure, PTFE, and temperature will change during PEMFC operation. Moreover, the PEMFC layer components are very thin with some of them being partially transparent. For some of the materials, the thermal conductivity is also non-isotropic. The challenges are different for each material and we present herein a short review of previous efforts in obtaining the thermal conductivity of the PEMFC component.

Based upon the available literature, it is fairly safe to state that the thermal conductivity

of the GDL is now starting becoming well understood. The most thorough review available on this topic is, to the author's knowledge, one by Zamel and Li (8), and the present review is in part also an extension of their work.

For the GDL, the in-plane and through-plane thermal conductivities are different. Because the in-plane electrical conductivity is several times larger than the through-plane electrical conductivity, it was first postulated (27–29) and later verified experimentally (14–16) that the in-plane thermal conductivities are several times larger than the through-plane ones. It was found that the in-plane thermal conductivities are five to ten times larger than the through-plane ones (mainly depending on the GDL compaction).

In through-plane thermal conductivity measurements, the thermal contact resistance, the bulk material thermal conductivity and the thickness change with the applied compaction pressure must be accounted for (11–13). In these measurements, one must separate the thermal contact resistance between the apparatus and the sample from the bulk material thermal resistance, which can lead to difficulties and reasonable assumptions must be made and accounted for. Both water and PTFE will affect the thermal conductivity of the GDL (10, 12, 13, 30, 31).

First, the thermal conductivity was measured *in-situ* in the fuel cells by embedding thermocouples between the MPL and the catalyst layers and determining the thermal conductivity from the heat sources, see Vie and Kjelstrup (9). The lack of precise knowledge of the location for the thermocouples reduced the precision with this approach. They determined the average thermal conductivity of the GDL (ETEK ELAT) and CL together to be  $0.2 \pm 0.1 \text{ W m}^{-1} \text{ K}^{-1}$ . The first *ex-situ* experiments of thermal resistance (of the sample and the contact to the apparatus) were reported by Ihonen et al. (32). Khandelwal and Mench (10) reported the first *ex-situ* measurements of GDL materials where the thermal conductivity and the thermal contact resistance to the apparatus was de-convoluted. In this study (10), the compression, and thus the actual thickness, was not measured and hence the precision of the reported values decreased. Ramousse et al. (33) used a similar approach. The first report on *ex-situ* measurements accounting all of the three parameters required by Fourier's law and as a function of compaction pressures was that of Burheim et al. (13). When correcting for the actual thickness due to the compression, the reported thermal conductivity values decrease by 5-20%. This can be seen as a direct consequence of Fourier's law (rewritten:  $k = \dot{q} \frac{\Delta x}{\Delta T}$ ), where reduction in thickness leads to reduced determined thermal conductivity. Perhaps the most important part of this study was that we demonstrated that the GDL-GDL contact thermal resistance is negligible and that therefore neglecting this when stacking materials is a valid approach for through-plane thermal conductivity measurements. Generally, these studies together suggested and agreed that at room temperature and for dry materials the through-plane thermal conductivity of an ELAT GDL is around  $0.2 \text{ W K}^{-1} \text{ m}^{-1}$ , a Sigracet GDL  $0.3\text{-}0.4 \text{ W K}^{-1} \text{ m}^{-1}$  and Toray GDL is  $0.3\text{-}0.8 \text{ W K}^{-1} \text{ m}^{-1}$ .

An important remark when it comes to the Toray GDLs, is that the thicker papers have higher thermal conductivity for the thicker materials (12). This can be attributed to the additional binder in the thicker materials as these consists of thinner GDLs that are "glued" together using a carbon binder (34). This must be accounted for when measuring thermal conductivity; if comparing four Toray-030's to one Toray-120 (being four binder glued

Toray-030's), it will appear that there is a large GDL-GDL contact resistance in the stack of Toray-030's, whereas it is in fact artificially increased conduction in the GDL-GDL regions inside the Toray-120's. This issue, of stacking Toray papers remains subject for discussion in the literature.

Changes in temperature lead to changes in thermal conductivity for GDLs. These were measured both for in- and through-plane thermal conductivity by Zamel et al. (16, 35). For the through-plane thermal conductivity with thickness controlled compression; it was found that at 16% compression (unknown compaction pressure) the thermal conductivity of the GDL, regardless of PTFE content, does not depend significantly on temperature (35). For the in-plane thermal conductivity, it was found that for PTFE free GDLs the thermal conductivity is lowered by  $\sim 50\%$  when comparing values measured at room temperature to values from measurements undertaken at  $60\text{ }^{\circ}\text{C}$  and higher (16). For the PTFE treated samples, the in-plane thermal conductivity is nearly unaffected in the range of  $-20$  to  $+120\text{ }^{\circ}\text{C}$ , respectively (16). This is similar to what Khandelwal and Mench reported for Nafion<sup>®</sup> (10).

Adding water to the GDL has been measured to increase the thermal conductivity of every type of GDL at room temperature by a factor between two and three (12). This is equivalent to what is reported when adding electrolyte to carbon electrodes in Li-ion batteries (36–38) and supercapacitors (39, 40). A recent study shows that the thermal conductivity increases gradually with the water content (25) and in particular during the first 10% of saturation. Saturation refers to the relative filling of the pore volume. The study shows that the increase in thermal conductivity appears the strongest as water first enters the GDL and then levels out as pores are filled with water. The absence of a linear behaviour was previously shown (12), but never quantified like this (25). The water was added upfront the measurement by submerging the samples in liquid water lowering the atmospheric pressure to get air bubbles out and by using an ultrasound device to redistribute the water. Thermal contacts to the apparatus were not accounted for. At elevated temperatures, i.e. temperatures above  $70\text{ }^{\circ}\text{C}$ , the effective thermal conductivity is increased further by the so called heat pipe effect. The heat pipe effect is imposed by a heat flux evaporating water at higher temperature and condensing water at a lower temperature and is also referred to as phase change induced flow (41, 42). The heat pipe effect is found to increase the through-plane thermal conductivity by 20-40% in the temperature range  $70\text{--}90\text{ }^{\circ}\text{C}$  (30). Moreover, Shum *et al.* investigated the thermal conductivity of the SGL10BA (GDL with some PTFE content) and found that the thermal conductivity remains very high during dry-out cycles even though the saturation became very low. In this study the thermal conductivity of the GDL containing water was done in combination with x-ray computer tomography (XCT). (26) The study showed that water is first removed from the larger pores and, at the end of the dry-out process, remains as very small droplets near the fibre-to-fibre contact regions. This is interesting as water is shown to appear as larger drops when first entering the GDL (43). It must therefore redistribute to the fibre-to-fibre contact regions afterwards and then remain there the longest during dry-out. These (fibre contact) regions are generally acknowledged for being the main mechanisms for heat conduction in GDLs and even very small additional water droplets in such spots contribute strongly to the GDL effective thermal conductivity. This is as instead of transferring heat through a fibre-to-fibre contact spot (point), one has a fibre-water contact region (volume). The study by Shum *et al.* showed that at the end of

the dry-out, the majority of the remaining droplets were 2-10  $\mu\text{m}$ , with smaller being more frequent than larger ones (26) and necessarily located near fibre to fibre contact points.

PTFE is, on the contrary to water, found to decrease the through-plane thermal conductivity of every type of GDL. (44) This is a common conclusion among all studies that includes varying the PTFE content. The common understanding in the literature appears to be that under the absence of PTFE and when a GDL is compressed, more “fibre-to-fibre” contacts are produced leading to an increase of the effective thermal conductivity. In the presence of PTFE, the uncompressed GDLs thermal conductivity is increased by PTFE conducting some heat between the carbon fibres (45). As soon as the GDL is compressed, the PTFE only inhibits more fibre to fibre contacts and then the effective through-plane thermal conductivity of the GDL is lowered, because of PTFE. This is observed even when the smallest portions of PTFE is added to the GDL.

Aged GDLs have reduced PTFE content which is shown to increase water retention inside the GDL rather than rejection from the surface (19, 46–48). Ageing of GDLs can be undertaken by either boiling the GDLs in oxygen rich water (19) or heating the GDLs in almost boiling hydrogen peroxide solutions (46, 47). By boiling GDLs in oxygen enriched water for up to 1000 hours, the thermal conductivity of dry GDLs remained constant whereas the thermal conductivity with water increased (19). During this ageing procedure, PTFE was partly removed and more water would retain, once rehydrated upon thermal conductivity measurements. This led to a slight increase in thermal conductivity. The difference in ageing and thermal conductivity of dry and wet GDL posts the question; from what regions is PTFE removed during ageing of GDLs? One alternative is that the PTFE is removed from fibre-to-fibre contact regions. Another alternative is the opposite, if it is systematically removed. On the one hand, PTFE is introduced by adding water with dispersed PTFE into the GDL and then dry out the water. From the dry-out study by Shum *et al.*, this means that PTFE should be mainly allocated in the fibre-to-fibre contact region. This indicates that when PTFE is removed, water will improve thermal conduction in these regions. On the other hand, the slight increase in wet thermal conductivity suggests that water is more active in the larger pore structures. Better studies of where and how the PTFE is removed during ageing using XCT is therefore needed along with more studies of thermal conductivity with higher control of saturation levels.

Nafion<sup>®</sup> is the most commonly used membrane in a PEMFC. One study shows that the thermal conductivity at room temperature increases linearly with water uptake, from 0.18 to 0.27  $\text{W K}^{-1} \text{m}^{-1}$  at water content of close to 0 and up to 22 water per sulphonic group (13). Another study showed that the thermal conductivity of a dry Nafion<sup>®</sup> decreases linearly with temperature, from 0.17 (room temperature) to 0.14 (65 °C) (10). The in-plane thermal conductivity of dry Nafion<sup>®</sup> was measured by Alzhami *et al.* (44), and found to decrease from 0.19  $\text{W K}^{-1} \text{m}^{-1}$  at 35°C to 0.14  $\text{W}^{-1} \text{K}^{-1} \text{m}$  at 65°C. Thus, for Nafion<sup>®</sup>, it can be interpreted that the in-plane thermal conductivity is not significantly different from the through-plane thermal conductivity.

The thermal conductivity of different MPL made for PEMFC was first investigated independently of any other fuel cell components by Burheim *et al.* (22). The value was found to vary between 0.06 and 0.10  $\text{W K}^{-1} \text{m}^{-1}$  at compaction pressures ranging from 5 to 16 bar. Despite that the MPL are among the thinnest layers of a PEMFC they ap-

pear with a thermal conductivity so low that they can still have an important effect on the overall temperature distribution in a PEMFC. A recent study by Thomas et al. showed that the temperature gradient across this layer contribute to water transport and also that this increase in temperature helps keeping the water in the MPL in a gas phase (20). Studies following up on MPL thermal conductivity to varouious degrees account for the integration with the substrate GDL (21, 23). The discussion revolves around whether the GDL and the MPL are integrated or not and what the implications of this is. If, as suggested in (23), this region is significant and has super high thermal conductivity, the MPL thermal conductivity of the MPL is  $0.1 \text{ W K}^{-1} \text{ m}^{-1}$  and less. If, as suggested in (21), the MPL can be treated as a single layer on top of the GDL and the GDL thermal conductivity is unaffected by any MPL intrusion, the MPL thermal conductivity is  $0.2 \text{ W K}^{-1} \text{ m}^{-1}$  and more. As a follow up in this study, Bock *et al.* tried to reeate the MPL-GDL composite material by filling an entire GDL with MPL in such way that the MPL would fill the GDL completely (49). This study showed that the thermal conductivity increases significantly, but not nearly as much as suggested in (23). It is unclear, what all the different MPLs were made from, which in principle could also affect the results. Several research questions regarding the composition and mechanisms in heat transfer in the MPL-GDL composite thus appears unanswered.

The MPL and the catalyst layers have many similarities and therefore it is interesting to investigate the thermal conductivity also of the CL, even though it can have a thickness of 10-30  $\mu\text{m}$ . At least three studies of thermal conductivity of CL thermal conductivity exists (24, 50, 51). Two of these studies looks at stand-alone catalyst layers. In the oldest study, the CL consisted of Pt nano particles on carbon black and ionomers equal in weight and the thermal conductivity is reported to range 0.07-0.11  $\text{W K}^{-1} \text{ m}^{-1}$  at 5-15 bar compaction pressure for the dry CLs (24). Doubling the ionomer amount or removing the Pt did not significantly affect the results. Adding water by condensation, however, appear to reduce the thermal resistivity by around a factor of two. The other study that experimentally measured and report CL thermal conductivity reported 0.21-0.24  $\text{W K}^{-1} \text{ m}^{-1}$  in the range of 5-15 bar compaction pressure for dry thermal conductivity (50). An important difference between the two studies is that the most recent one (50) used graphitised carbon, rahter than the non-graphitised of the former study (24). Another difference is that the former of these two studies used an air brush in manufacturing the CL whereas the latter used a roller. These two differences can explain the difference in compressibility aand also in thermal conductivity, as graphitisation is proven to improve thermal conductivity of porous carbon by a factor of four (36). The measurements by Ahadi *et al.* (50) was supported by a numerical model (51). Clearly, also within CL thermal conductivity, several research questions remain unanswered.

## Model Description

In order to illustrate how the understanding of internal temperature distribution has developed alongside the knowledge of thermal conductivity, a 2D thermal model is developed using the commercial software Comsol Multiphysics 4.2.

**TABLE I.** The heat sources used for the model in this paper.

Material	$\dot{Q}_i \cdot \delta_i / \text{W m}^{-2}$ (2, 55)
Anode	$0.001 j + \frac{T\Delta S}{zF} j \cdot 0.80$
Cathode	$\left(0.45 + 0.06 \ln \frac{j}{10^4}\right) j + \frac{T\Delta S}{zF} j \cdot 0.2$
Membrane $j = 10\,000 \text{ A m}^{-2}$	$\frac{\delta_i}{8.7} j^2$ $E^{cell} = 0.67 \text{ V}$

## Geometry

The presented model uses two geometries that are depicted in Fig. 1. The figure depicts a cross section of a PEMFC single cell, where the different layers (GDL, MPL, CL and membrane) are sandwiched between two polarisation plates (solid grey) containing gas feed channels (open squares). The model is based on the assumption that transport phenomena is the same along the channel length and that the variations change repeatedly along the direction of the membrane length. This creates repeated temperature distribution where mirror symmetric lines can be in the address perpendicular to the membrane length, both under the middle of the feed channel and under the middle of the part of the polarisation plate commonly referred to as rib or land. These two mirror symmetry lines are indicated with blue lines in Fig. 1. It is the light red coloured area between these two lines that defines the modelled region in this study.

The difference between the two geometries is only whether or not the MPL intrudes into the GDL, which it does in the right sketch. The MPL is depicted using a transparent solid grey. The reason why these two illustrations are given is to show that once including for the GDL-MPL composite region, the GDL region becomes thinner. Moreover, as the MPL intrudes into the GDL, only the through-plane thermal conductivity can be expected to change.

The gas channels in the model are considered to be squared, 1mm by 1mm, and so is the rib (land) too. These can be different in different fuel cells, however the present configuration represents a realistic and typically applied dimension. Moreover, one can see that the GDL intrudes into the gas channel in Fig. 1. Although this is what happens in most cases during compression (52, 53), these effects are not included in the modelling. This goes for neither the geometry intrusion effect or potential thermal conductivity changes of the GDL under the gas channel. In other words, the present model considers the GDL to be uniformly compressed.

## Heat Sources

Non-isothermal mathematical models have become more of a standard for PEMFC over the past decade, see e.g. Bapat and Thynell (7) and Zhang and Khandlikar (54). In this paper we present a model that accounts for temperature gradients induced by standard heat sources in order to show the importance of the knowledge development in thermal conductivity values.

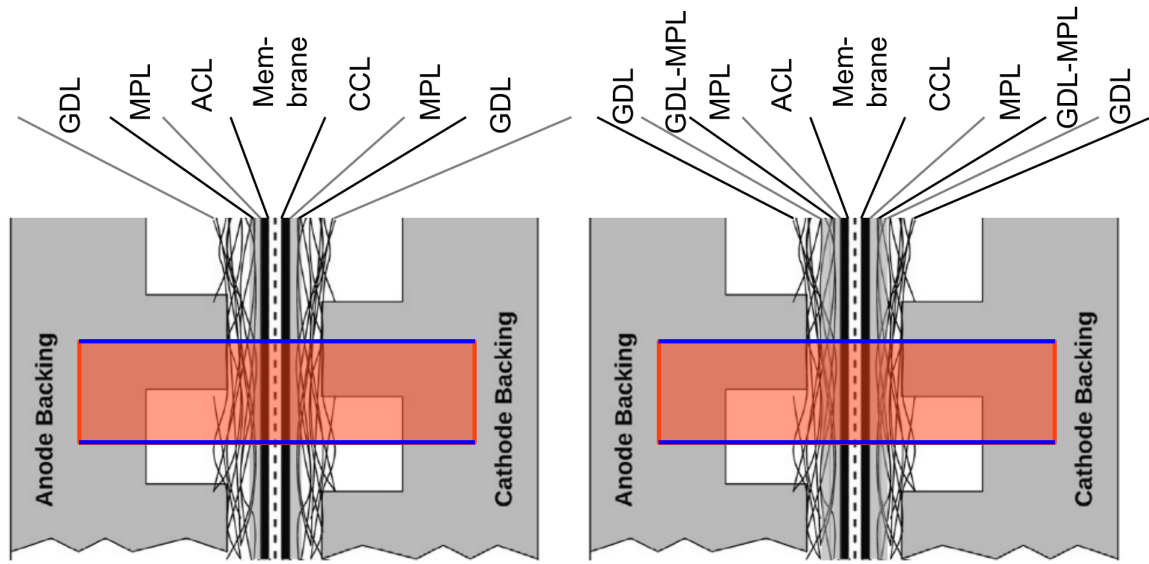


Figure 1. The geometry of the cell design modelled, accounting for MPL-on-top geometry (left) and MPL-GDL composite region (right).

The model is developed in the commercial software Comsol 4.2a which is set to solve

$$\nabla(k_i \nabla T) + \dot{Q}_i = 0 \quad [1]$$

where  $k_i$  is the thermal conductivity and  $\dot{Q}_i$  is the volumetric heat source for region  $i$  as given in Table I. The model was solved using Dirichlet (constant temperature) boundary conditions at the end (red lines Fig. 1) and Robin (insulating Neuman) at the symmetry lines (dark blue Fig. 1). In this model, each layer is set to represent an element in the FEM model, as Eq. 1 requires no domain sub-meshes when second order mesh (quadratic math) is chosen. The model considers evenly distributed heat generation for each of the layers described in Table I.

### Thermal Conductivity Selections

Five selected combinations of thermal conductivities are chosen to illustrate, not only the historical knowledge development, but also relevant cases of operation and cell design. The denominator is that the polarisation plate is considered kept at 80 °C and that the membrane current density is considered uniform. The compaction pressure refers to around ten bar uniform compaction pressure. The thermal conductivity and layer thickness of the five cases are given in Table II. The five cases are described in the following.

The Base Case. The base case represents a dry PEMFC in operation using knowledge of thermal conductivity as it was almost ten years ago. This includes for a thermal contact resistance between the GDL and the rib (under land) equivalent to 10  $\mu\text{m}$  of air. The thermal conductivity of the MPLs and the CLs were not determined at this point and assumed to be similar to what was known for the GDL. The rest of the values are selected straight forward from what is tabulated in the literature.

**TABLE II.** The thermal conductivity values used for the base case model.

Material	$k / \text{W K}^{-1}\text{m}^{-1}$	$\delta_i / \mu\text{m}$	References
Base Case:			
Polarisation plates	200	$\geq 100$	
GDL Thermal Contact	0.025	10	(11, 12)
GDL - ETEC/SGLBA-type	0.35	250	(9, 13, 44, 56)
GDL - in-plane	2	$\infty$	(14–16)
MPL - on top	0.3	50	(19–21)
Anode CL	0.3	10	By tradition (6, 18)
Cathode CL	0.3	20	By tradition (18)
Nafion ( $\lambda = 15$ )	0.23	50	(13)
Thin Layer:			
MPL - on top	0.09	50	(22)
Anode CL	0.09	10	(24)
Cathode CL	0.09	20	(24)
MPL integration:			
GDL - ETEC/SGLBA-type	0.35	150	(12, 13)
GDL-MPL-integration	10	100	(23)
MPL - on top	0.09	50	(22)
Anode CL	0.09	10	(24)
Cathode CL	0.09	20	(24)
Water:			
GDL Thermal Contact	0.56	10	(11, 12)
GDL - ETEC/SGLBA-type	0.5	150	(12, 13)
GDL-MPL-integration	15	100	(23)
MPL - on top	0.18	50	(22)
Anode CL	0.18	10	(24)
Cathode CL	0.18	20	(24)
Nafion ( $\lambda = 22$ )	0.26	50	(13)
Wet Toray:			
GDL Thermal Contact	0.56	7	(11, 12)
GDL - Toray090	1.5	150	(10, 12, 13)
GDL-MPL-integration	15	100	(23)
MPL - on top	0.18	50	(22)
Anode CL	0.18	10	(24)
Cathode CL	0.18	20	(24)
Nafion	0.26	50	(13)

Importance of the Thin Layers - CL and MPL. The thin layer model includes for the knowledge that thermal conductivity of the MPL (on top) and the CL have much lower thermal conductivity than what was initially assumed. Model wise, this modification consists of replacing the thermal conductivity values of the regions of MPL (on top) and CL.

The MPL GDL Integration Region. The discovery that the region where the MPL intrudes into the GDL has much higher thermal conductivity is accounted for by separating the GDL into two bodies, one outer (near the polarisation plate) and one inner (near the MPL). The outer body has its thermal conductivity remaining, whereas the inner has its through-plane thermal conductivity increased by a factor of more than ten, see Table II.

Effect of Water. Presence of liquid water changes the thermal conductivity of all the components and thermal resistances of the PEMFC. The thermal contact between the polarisation plate and the GDL, earlier described as a  $10\mu$  layer of air, is now better represented by a  $10\mu\text{m}$  layer of water. The thermal conductivity of the GDL, MPL and CL close to double and the thermal conductivity of the membrane increase its thermal conductivity just slightly due to increased water uptake (by the Schroedinger paradox(57)).

Toray and Water. The energy dissipated as heat in a PEMFC must travel through the GDL and therefore this is a very important component for cooling the MEA. The GDL with the highest thermal conductivity is the Toray based GDL, here selected as the Toray-090, containing liquid water. This case represents the set of highest thermal conductivities.

### **Results: Influence on Internal Temperature Profiles**

Figure 2 gives the modelled temperature profiles under the land or rib (upper) and under the gas channel (lower). Both axis windows (distance vs. temperature) are the same and one can immediately see that it is hotter under the gas channel than under the rib. The next immediate difference, perhaps, is the difference in the temperature gradients between the cases containing (liquid) water and not, where the cooling effect from having liquid water is shown. A remarkable difference is that between the two most extreme cases the maximum temperature difference in the PEMFC ( $\Delta_{max}T$ ) are 2 and 11 °C. Depending on the knowledge of the component thermal conductivity and state of water, the temperature difference from the temperature of the polarisation plate will change by a factor larger than five! That is close to one order of magnitude in difference.

The difference between the three first cases (base case, thin layer, and GDL-MPL-composite) is interesting as the first and the last ends up with the same maximum temperature. Initially it might appear insignificant, but this indicates that the MPL has a role in providing a temperature gradient that removes liquid water at the electrodes by vaporisation, that is, the higher temperature allows for higher partial pressure of water vapour and in turn less likelihood of local flooding. The other part that is interesting when studying the base case versus the GDL-MPL integration, is that one can see that comparing a GDL with no MPL and a GDL with MPL, it will appear that the GDL has the same thermal conductivity as the MPL. This is as the effective thermal conductivity is the same for both (GDL vs. GDL+MPL). It is the knowledge that the MPL has much lower thermal conductivity than a GDL (thin layer model) that allows for more detailed studies of what is going on in terms of transport phenomena in this region. The present model is not advanced enough to pursue these processes in greater detail, however insight to potential differences in these three gradients indicate problems worth pursuing further.

The difference between under land (rib) and under channel stems from that the heat under the channel has further distance to travel and that the heat flux via an in-plane path increases towards the land (build-up by accumulation). It is these two effects that leads to higher temperature under the gas channel. The heat transport in the gas channel was modelled using a Newtonian heat transport coefficient of  $50\text{ W K}^{-1}\text{ m}^{-1}$ , and although this is

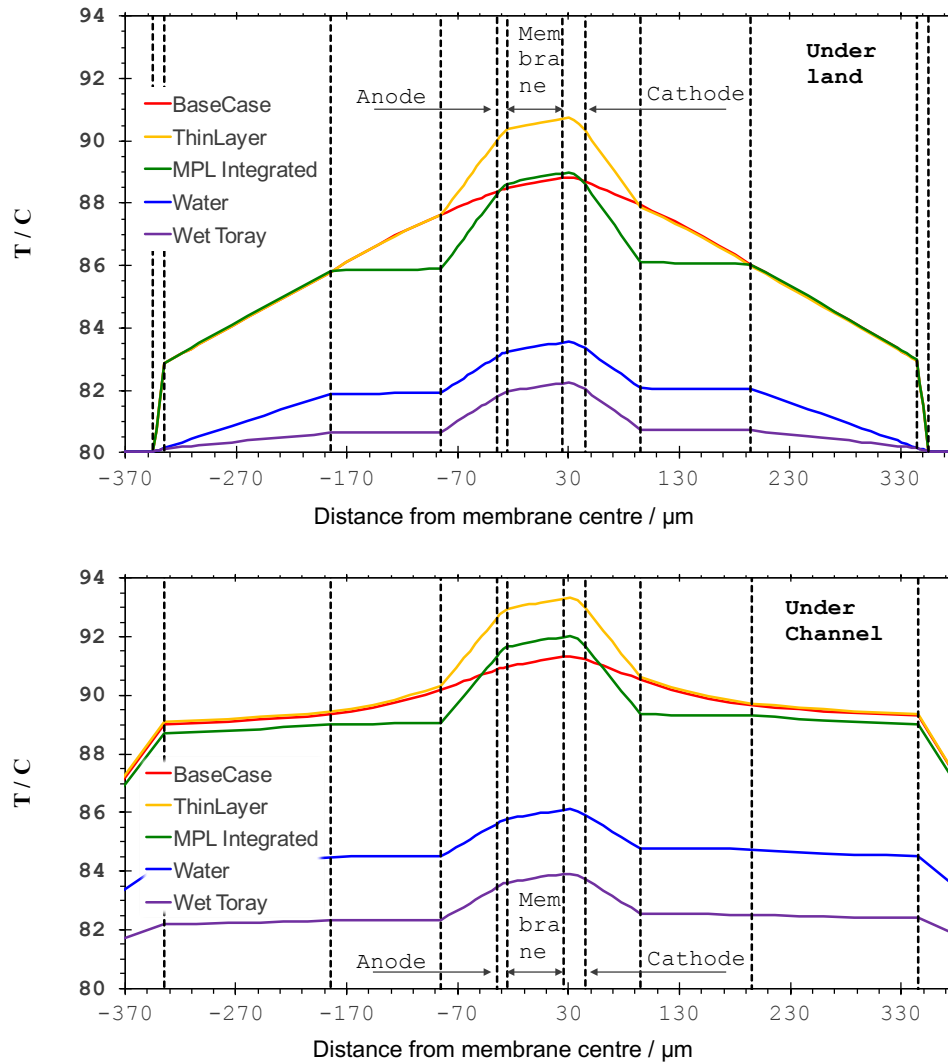


Figure 2. Through-plane temperature profiles from the five modelled cases; Upper figure shows the temperature gradients under the land (or rib) whereas the lower shows the one under the gas feed channel. See Fig. 1.

a very high heat transport coefficient for air (58) in the presented model, this is not sufficient to improve the heat transport by convection through the gas channels - only change the temperature profiles near the GDL and polarisation plate surfaces. The temperature gradients in the PEMFC under the gas channel and inside the gas channels is shown in Fig. 3. Including vortex shedding induced by the GDL fibres will obviously change the part of this analysis that covers the heat transfer in the gas channel.

Temperature distributions and thermal conductivity are related by Fourier's law. When the thermal conductivity lowers or the heat increases for a fixed geometry, the gradients and maximum temperature difference increases accordingly. Evaluation a PEMFC, the design is set up to increase its performance in terms of power density, ultimately leading to higher heat dissipation and in turn larger temperature gradients. The chosen kinetics and cell potential are moderate, if considering that fuel cells capable of twice the exchange current density and half the ohmic resistance at the same cell voltage are available. Such

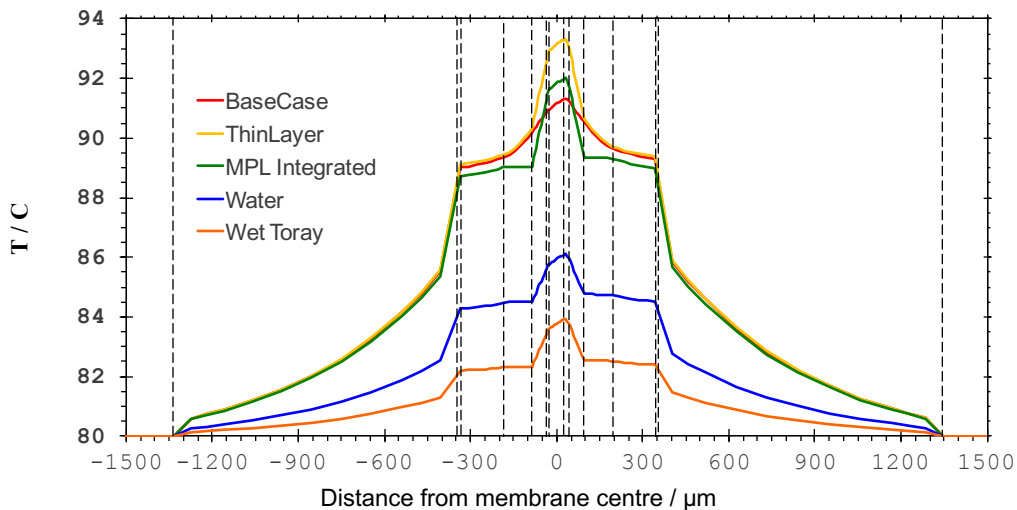


Figure 3. Temperature profiles under the gas channels also including the gradients inside the gas channel.

improvement would double the proposed current density and increase power density and heat density by a factor of 75% - in turn increasing the modelled temperature gradients by a factor of 75%. In this perspective, the presented model represents moderate internal temperature gradients

The current density along the membrane length (see Fig. 1) is rarely uniform, like suggested in the present model. When using serpentine gas flow channels, convection under land (rib) redistributes the current density to much higher under land than under the gas channel and when using parallel flow channels the current density is redistributed to be much higher under the gas channels than under land (27, 59, 60). Whereas the first (serpentine) will make the two selected temperature profiles more similar the latter will intensify the maximum temperature under the channel further. In this perspective, the presented thermal model represents an intermediate of different cell designs. The presented model is thus moderate in terms of cell performance and cell design when showing the temperature gradients in Fig. 2-3.

The effect of uneven compression is also not accounted for. The compaction pressure is larger under land (rib) than under the gas channel. Introducing effects like this to a thermal model will, in a similar manner to the current density redistribution from a parallel gas channel, make the temperature gradients under land decrease and under the gas channel increase. However, since the in-plane thermal conductivity is tenfold the through-plane thermal conductivity, uneven compression effects are more likely to affect the under land temperature gradient much more than the under gas channel one. Moreover, the under land region is also where water is most likely to accumulate by condensation, as is shown using neutron imaging (61). All over, the presented model only shows the changes imposed by increased thermal conductivity knowledge development relative to an already present understanding of the temperature gradients. In other words, although the model represents a moderate and realistic picture of PEMFC temperature gradients - its main purpose here is to illustrate how knowledge development over a decade changes our understanding of

internal temperature gradients of a PEMFC.

## Conclusion

The knowledge of thermal conductivity of PEMFC materials has grown a lot over the past ten years in terms of anisotropy, compaction pressure dependency, PTFE content variations, and water contribution. Depending on what type of materials that are used, what state water is in and gas channel design the maximum temperature difference to expected can change by more than a factor of ten.

Although, the thermal conductivity properties are starting to become well understood, several gaps in knowledge are addressed. This covers in particular water contributions during humidity cycling, MPL-GDL integration, and MPL material compositions.

## References

1. O. S. Burheim. *Engineering Energy Storage*. Academic Press, Elsevier, 1st edition, (2017). ISBN 9780128141007.
2. O. Burheim, P.J.S. Vie, S. Møller-Holst, J.G. Pharoah, and S. Kjelstrup. *Electrochim. Acta*, **5**:935–942, (2010).
3. O. S. Burheim and J. G. Pharoah. *Current Opinions in Electrochem.*, **XX**:XXX–XXX, (Submitted 2017).
4. F. Nandjou, J.-P. Poirot-Crouvezier, M. Chandesris, J. F. Blachot, C. Bonnaud, and Y. Bultel. *ECS Trans.*, **66**(25):1–12, (2015).
5. S.J.C. Cleghorn, D.K. Mayfield, D.A. Moore, G. Rusch, T.W. Sherman, N.T. Sisifo, and U. Beuscher. *J. Power Sources*, **158**:446–454, (2006).
6. S. G. Kandikar and Z. Lu. *J. Fuel Cell Sci. and Technol.*, **6**:04401–1–13, (2009).
7. C.J. Bapat and S.T. Thynell. *ASME, J. Heat Transfer*, **129**:1109–1118, (2007).
8. N. Zamel and Xiangou Li. *Progress in Energy and Combustion Sci.*, **39**:146, (2013).
9. P.J.S. Vie and S. Kjelstrup. *Electrochim. Acta*, **49**:1069–1077, (2004).
10. M. Khandelwal and M. M. Mench. *J. Power Sources*, **161**:1106–1115, (2006).
11. J. Ramousse, O. Lottin, S. Didierjean, and D. Maillet. *Int. J. of Thermal Sci.*, **47**:1–6, (2008).
12. O. Burheim, H. Lampert, J.G. Pharoah, P.J.S. Vie, and S. Kjelstrup. *J. Fuel Cell Sci. Technol.*, **8**:021013–1–11, (2011).
13. O. Burheim, P.J.S. Vie, J.G. Pharoah, and S. Kjelstrup. *J. Power Sources*, **195**:249–256, (2010).
14. E. Sadeghi, N. Djilali, and M. Bahrami. *J. Power Sources*, **196**:3565–3571, (2011).
15. P Teertstra, G Karimi, and X Li. *Electrochim. Acta*, **56**:1670–1675, (2011).
16. N. Zamel, E. Litovsky, S. Shakhshir, X. Li, and J. Kleiman. *Appl. Energy*, **88**:3042–3050, (2011).
17. N Alhazmi, MS Ismail, DB Ingham, KJ Hughes, L Ma, and M Pourkashanian. *J. Power Sources*, **241**:136–145, (2013).
18. J.G. Pharoah and O.S. Burheim. *J. Power Sources*, **195**:5235–5245, (2010).

19. O. S. Burheim, G. Ellila, J. D. Fairweather, A. Labouriau, S. Kjelstrup, and J. G. Pharoah. Ageing and thermal conductivity of porous transport layers used for pem fuel cells. *J. Power Sources*, **221**:356–365, (2013).
20. A Thomas, G Maranzana, S Didierjean, J Dillet, and O Lottin. *Int. J. of Hydrogen Energy*, **39**(6):2649–2658, (2014).
21. M. Andisheh-Tadbir, E. Kjeang, and M. Bahrami. *J. Power Sources*, **296**:344–351, (2015).
22. O. S. Burheim, H. Su, S. Pasupathi, J. G. Pharoah, and B. G. Pollet. *Int. J. Hydrogen Energy*, **38**:8437 – 8447, (2013).
23. O. S. Burheim, G. A. Crymble, R Bock, N. Hussain, S. Pasupathi, A. du Plessis, S. le Roux, F. Seland, H. Su, and B. G. Pollet. *Int. J. Hydrogen Energy*, **46**:16775–16785, (2015).
24. O. S. Burheim, H. Su, H. H. Hauge, S. Pasupathi, and B. G. Pollet. *Int. J. Hydrogen Energy*, **39**(17):9397–9408, (2014).
25. G. Xu, J. M. LaManna, and M. M. Mench. *J. Power Sources*, **256**:212–219, (2014).
26. A. D. Shum, D. Y. Parkinson, X. Xiao, A. Z. Weber, O. S. Burheim, and I. V. Zenyuk. *Electrochim. Acta*, **XX**:XXX–XXX, (Revised 2017).
27. J.G. Pharoah, K. Karan, and W. Sun. *J. Power Sources*, **161**:214–224, (2006).
28. F. Danes and J. Bardou. *Revue Generale de Thermique*, **36**:200–208, (2008).
29. E. Sadeghi, M. Bahrami, and N. Djilali. *J. Power Sources*, **179**:200–208, (2008).
30. Y Wang and M. Gundevia. *Int. J. Heat Mass Transf.*, **60**:134–142, (2013).
31. Hamidreza Sadeghifar, Ned Djilali, and Majid Bahrami. *J. Power Sources*, **248**(0):632 – 641, (2014).
32. J. Itonen, M. Mikkola, and G. Lindhberg. *J. Electrochem. Soc.*, **151**:A1152–A1161, (2004).
33. J. Ramousse, O. Lottin, S. Didierjean, and D. Maillet. *J. Power Sources*, **192**:435–441, (2009).
34. Z Fishman, J Hinebaugh, and A Bazylak. *J. Electrochem. Soc.*, **157**(11):B1643–B1650, (2010).
35. N. Zamel, E. Litovsky, S. Shakhshir, X. Li, and J. Kleiman. *Int. J. Hydrogen Energy*, **36**:12618–12625, (2011).
36. O. S. Burheim, M. A. Onsrud, J. G. Pharoah, F. Vullum-Bruer, and P. J. S. Vie. **58**: Accepted, (2014).
37. F. Richter, S. Kjelstrup, P-J.S. Vie, and O. S. Burheim. *J. Power Sources*, **359**:592–600, (2017).
38. F. Richter, S. Kjelstrup, P-J.S. Vie, and O. S. Burheim. *Electrochim. Acta*, **XX**:XXX–XXX, (Accepted July 2017).
39. O. S. Burheim, M. Aslan, J. S. Atchison, and V. Presser. *J. Power Sources*, **246**:160 – 166, (2014).
40. HH Hauge, V Presser, and O Burheim. *Energy*, **78**:373–383, (2014).
41. S. Kim and M.M. Mench. *J. Electrochem. Soc.*, **156**:B353–B362, (2009).
42. A. Z. Weber and J. Newman. *J. Electrochem. Soc.*, **153**(12):A2205–A2214, (2006).
43. I. V. Zenyuk, D. Y. Parkinson, G. Hwang, and A. Z. Weber. *Electrochem. Communications*, **53**:24–28, (2015).
44. N. Alhazmi, M.S. Ismail, D.B. Ingham, K.J. Hughes, L. Ma, and M. Pourkashanian. *J. Power Sources*, **241**(0):136 – 145, (2013).

45. J. Yableckia, A. A. Nabovati, and A. Bazylak. *J. Electrochem. Soc.*, **159**:B647–B653, (2012).
46. P. K. Das, A. Grippin, A. Kwong, and A. Z. Weber. *J. Electrochem. Soc.*, **159**(5): B489–B496, (2012).
47. J. D. Fairweather, D. Spornjak, A. Z. Weber, D. Harvey, S. Wessel, D. S. Hussey, D. L. Jacobson, K. Artyushkova, R. Mukundan, and R. L. Borup. *J. Electrochem. Soc.*, **160**(9):F980–F993, (2013).
48. F.A. de Bruijn, V. A. T. Dam, and G.J.M. Janssen. *Fuel Cells*, **08**:1–22, (2008).
49. R. Bock, A. Shum, T. Khoza, F. Seland, N. Hussain, I. V Zenyuk, and O. S. Burheim. *ECS Trans.*, **75**(14):189–199, (2016).
50. M. Ahadi, M. Tam, M. S. Saha, J. Stumper, and M. Bahrami. *J. Power Sources*, **354**: 207–214, (2017).
51. M. Ahadi, A. Putz, J. Stumper, and M. Bahrami. *J. Power Sources*, **354**:215–228, (2017).
52. JP James, H-W Choi, and JG Pharoah. *Int. J. Hydrogen Energy*, **37**(23):18216–18230, (2012).
53. I. V. Zenyuk, D. Y. Parkinson, L. G. Connolly, and A. Z. Weber. *J. Power Sources*, **328**:364–376, (2016).
54. G. Zhang and S. G. Kandlikar. *Int. J. Hydrogen Energy*, **37**:2412–2429, (2012).
55. O. Burheim, S. Kjelstrup, J.G. Pharoah, P.J.S. Vie, and S. Møller-Holst. *Electrochim. Acta*, **5**:935–942, (2011).
56. Grant Unsworth, Nada Zamel, and Xianguo Li. *Int. J. Hydrogen Energy*, **37**:5161 – 5169, (2012).
57. Lisa M. Onishi, John M. Prausnitz, and John Newman. *The J. Phys. Chem. B*, **111**(34): 10166–10173, (2007).
58. Todd M Bandhauer, Srinivas Garimella, and Thomas F Fuller. *J. Electrochem. Soc.*, **158**(3):R1–R25, (2011).
59. D. Harvey, J.G. Pharoah, and K. Karan. *J. Power Sources*, **179**:209–219, (2008).
60. S.A. Reum, M. Freunberger, A. Wokaun, and F.N. Buchi. *J. Electrochem. Soc.*, **156**: B301–B310, (2009).
61. A. Turhan, K. Heller, J. S. Brenizer, and M. M. Mench. *J. Power Sources*, **180**:773 – 783, (2008).